



UNIVERSITY OF LEEDS

This is a repository copy of *Liquid crystalline phases of linear alkylbenzene sulphonate in spray-dried detergent powders studied by small-angle X-ray scattering, TEM, and ATR-IR spectroscopy*.

White Rose Research Online URL for this paper:  
<https://eprints.whiterose.ac.uk/171664/>

Version: Accepted Version

---

**Article:**

Farshchi, A, Sadeghpour, A [orcid.org/0000-0002-0475-7858](https://orcid.org/0000-0002-0475-7858), Rappolt, M [orcid.org/0000-0001-9942-3035](https://orcid.org/0000-0001-9942-3035) et al. (5 more authors) (2021) Liquid crystalline phases of linear alkylbenzene sulphonate in spray-dried detergent powders studied by small-angle X-ray scattering, TEM, and ATR-IR spectroscopy. *Colloids and Surfaces A: Physicochemical and Engineering Aspects*, 614. 126130. ISSN 0927-7757

<https://doi.org/10.1016/j.colsurfa.2020.126130>

---

© 2021, Elsevier B.V. This manuscript version is made available under the CC-BY-NC-ND 4.0 license <http://creativecommons.org/licenses/by-nc-nd/4.0/>.

**Reuse**

This article is distributed under the terms of the Creative Commons Attribution-NonCommercial-NoDerivs (CC BY-NC-ND) licence. This licence only allows you to download this work and share it with others as long as you credit the authors, but you can't change the article in any way or use it commercially. More information and the full terms of the licence here: <https://creativecommons.org/licenses/>

**Takedown**

If you consider content in White Rose Research Online to be in breach of UK law, please notify us by emailing [eprints@whiterose.ac.uk](mailto:eprints@whiterose.ac.uk) including the URL of the record and the reason for the withdrawal request.



[eprints@whiterose.ac.uk](mailto:eprints@whiterose.ac.uk)  
<https://eprints.whiterose.ac.uk/>

# **Liquid Crystalline Phases of Linear Alkylbenzene Sulphonate in Spray-Dried Detergent Powders Studied by Small-Angle X-ray Scattering, TEM, and ATR-IR Spectroscopy**

Amin Farshchi<sup>1\*</sup>, Amin Sadeghpour<sup>2,3</sup>, Michael Rappolt<sup>2</sup>, Hossam Tantawy<sup>4</sup>,  
Joel Caragay<sup>4</sup>, Eric S. J. Robles<sup>4</sup>, Ali Hassanpour<sup>1</sup> and Andrew Bayly<sup>1\*</sup>

<sup>1</sup>*School of Chemical and Process Engineering, University of Leeds, Leeds, LS2 9JT, UK*

<sup>2</sup>*School of Food Science and Nutrition, University of Leeds, Leeds, LS2 9JT, UK*

<sup>3</sup>*Biomaterials Science Centre, Department of Biomedical Engineering, University of Basel,  
Allschwil CH-4123, Switzerland*

<sup>4</sup>*The Procter & Gamble Company, Newcastle Innovation Centre, Newcastle-Upon-Tyne  
NE12 9TS, United Kingdom*

\*Corresponding authors: Amin Farshchi, E-mail: [A.Farshchi@tees.ac.uk](mailto:A.Farshchi@tees.ac.uk)

Andrew Bayly, E-mail: [A.E.Bayly@leeds.ac.uk](mailto:A.E.Bayly@leeds.ac.uk)

## Introduction

Spray drying is the most extensively used process to produce laundry detergent powders, whereby heterogeneous slurry can be transformed into low-density powders referred to as “blown powders”. The resulting spray-dried powders commonly contain thermally stable and chemically compatible ingredients, *e.g.* surfactant, fillers and builders, and comprise 30-90 wt% of the finished products. Other additives which cannot be processed during the spray drying, such as enzymes, bleaches, foam regulators and fragrances are subsequently added in post-tower operations.

Blown powder was previously shown to possess a complex composite structure due to the multi-phase nature of the starting slurry and its evolution during the drying process [1]. A typical structure of these granules, in macro-scale, can be seen in Fig. 1, which highlights the presence of three distinct phases including remaining undissolved inorganic salts, matrix phase and porosity. The matrix is formed from the dried slurry liquid phases and is a composite structure of binders, *e.g.* sodium silicate, dried surfactant liquid crystalline phase and sub-micron scale crystallites of sodium sulphate. The initial water content of detergent slurries plays a crucial role in determining the volume fraction of the matrix phase. In general, the greater the water content, the lower the amount of remaining undissolved inorganic salt phase within the granules, and hence the greater is the matrix phase. Air is also dispersed in this matrix at two length scales, large vacuoles, driven by ‘puffing’ *i.e.* water boiling, and micro-scale porosity, which evolves during the crystallisation of the drying matrix. The amount, size and distribution of these three phases may have a considerable effect on the functional properties, *e.g.* flow behaviour, storage stability and dissolution rate, of the final product. Improvement of these functional properties requires a better fundamental understanding of the granular structure. This consequently leads to an appropriate selection of slurry formulation and spray drying operating conditions.

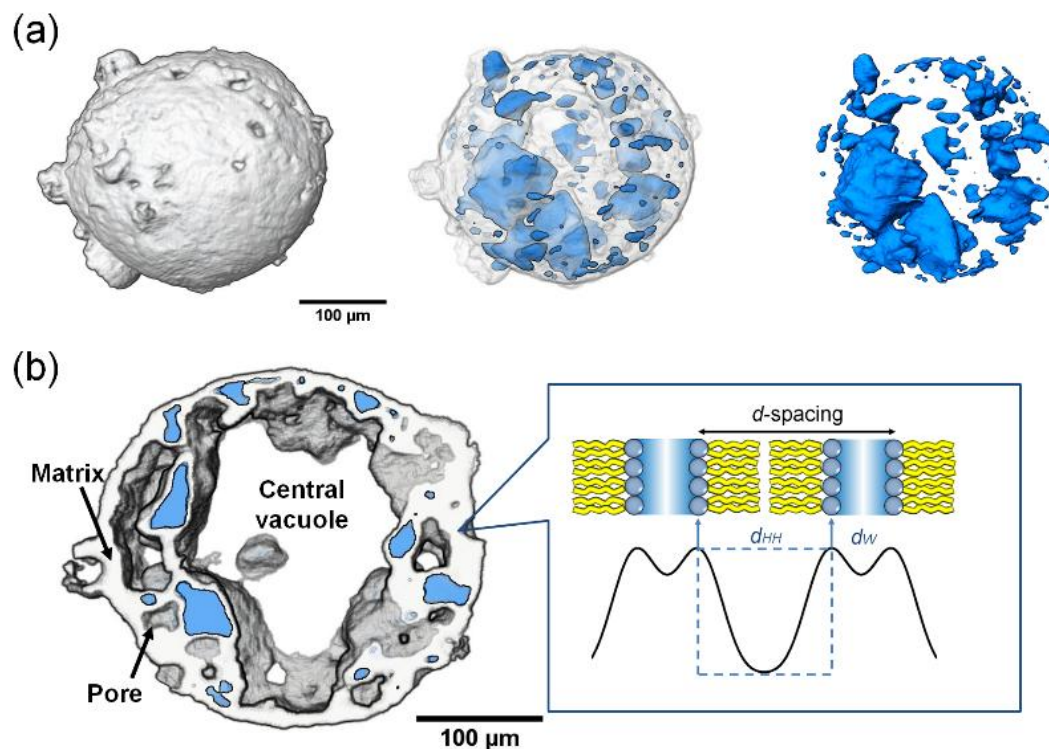


**Figure 1.** (a) A 3D X-ray micrograph (Voxel size:  $1.74\ \mu\text{m}$ ) of a typical detergent granule (equivalent diameter:  $287.8\ \mu\text{m}$ ) produced from a silicate-containing slurry, displayed with increasing matrix transparency to show morphological properties and distribution of initially undissolved crystals of sodium sulphate (blue particles); and (b) shows its 3D central cross section ( $68\ \mu\text{m}$  thick) illustrating the distribution of pores, and sodium sulphate crystallites (left), and a typical electron density profile of lamellar liquid-crystalline phases ( $L_\alpha$ ) is illustrated in a cartoon (right), showing the parameters of lamellar  $d$ -spacing, water layer thickness ( $d_w$ ) and bilayer thickness ( $d_{HH}$ ).

As mentioned earlier, the matrix phase contains dehydrated liquid crystalline surfactant. Anionic surfactants are widely used in most surfactant-based detergent formulations. Laundry detergent powders predominantly contain sodium salt of linear alkylbenzene sulphonate (NaLAS). In general, amphiphilic molecules such as linear alkylbenzene sulphonate (LAS), in the presence of water, tend to arrange into various ordered self-assembled structures depending on the concentration and molecular shape. NaLAS can be industrially synthesised by alkylation and sulphonation of benzene. A commercial NaLAS consists of a range of homologs and phenyl isomers with different alkyl chain lengths (typically  $C_{10}$  to  $C_{14}$ ) and

substitution of the benzene ring at any position of alkyl chain except for the terminal methyl groups, Fig. 2 [2, 3].

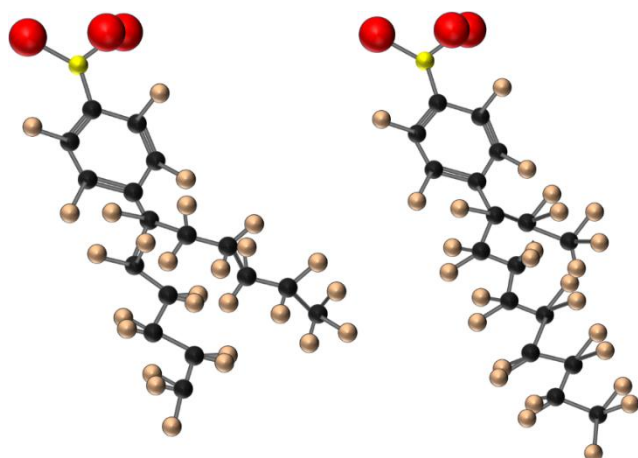


**Figure 2.** Schematic representation of two positional 6- and 3-phenyl isomers of linear sodium alkylbenzene-sulphonate (NaLAS), respectively [4].

Amphiphilic molecules with varied alkyl chain lengths may adopt various ordered self-assembled structures: micellar, hexagonal, cubic and/or lamellar phases ( $L_\alpha$ ), depending on the molecular packing parameter [5], and consequently this influences their properties, *e.g.* rheology and optical properties [6]. However, studies on the phase diagrams of commercial LAS in aqueous systems have revealed that unlike typical surfactants, NaLAS molecules tend to form only micellar and lamellar phases due to its unique chemical structure and phenyl isomer distribution. Above 15°C, only micellar phase at low concentrations below around 20% is observed but below this temperature, multi-lamellar vesicles are formed. Above 15°C, a broad multi-phase region is formed in the composition range of ~ 20 – 70% NaLAS, where one or more lamellar phases ( $L_\alpha$ ) coexist with a micellar ( $L_1$ ) phase [7]. At this multi-phase region, heating in a temperature range of ~ 35 – 65 °C can lead to the formation of multi-lamellar phases. At higher concentrations above around 65% NaLAS, only multi-lamellar phases are present over a broad temperature range; typically 0 – 100 °C [4]. Finally, in the concentrated region, around above 80% NaLAS, solid multi-lamellar phases can be

identified, coexisting with liquid crystalline phases [8]. The addition of salting-out electrolytes, *e.g.* sodium sulphate, to the aqueous systems of commercial NaLAS favours the transformation of isotropic micellar solution to lamellar phases at lower NaLAS concentrations. This phase transformation at lower concentrations is induced by the binding of the cations to the micellar surface, which therefore screens electrostatic repulsions between head groups. This leads to the aggregation of micelles, and hence to the formation of lamellar structures [7]. Rafique, et al. [9] investigated the shape, dimensions, and transformation pathways of micelles of linear sodium alkylbenzene sulphonate in aqueous systems using Small Angle Neutron Scattering (SANS) and showed that at fixed NaLAS concentration, salt addition causes spherical micelles to grow into cylindrical micelles, and then multilamellar vesicles (MLVs).

The self-assembled structures of NaLAS, however; have not been analysed well in spray-dried detergent powders so far. In our previous work on the multi-scale structure of detergent powders, the small-angle X-ray scattering (SAXS) results revealed the presence of multi-lamellar liquid crystalline phases, which were shown to be influenced by the initial chemical composition of the slurries. Silicate-induced structural changes in lamellae was observed in our previous work [1], and it was shown that relatively long *d*-spacings of multi-lamellae disappeared in the presence of sodium silicates, leading to a more uniform system with stronger Bragg peaks. It has been demonstrated that hygroscopic binders such as sodium silicates play a key role in the response of the detergent powders to increased relative humidity of the surrounding air, particularly during storage in humid conditions [10]. This hygroscopic characteristic may potentially cause changes in the lamellar structure; membrane and hydration water layer thicknesses. Nevertheless, the nature of these structural changes has not been well understood and remains an interesting problem which merits further investigation.

This study reports, for the first time, a detailed structural analysis of the NaLAS lamellae in detergent powders via Fourier analysis of SAXS data of two simplified, model formulations. One formulation contained only sodium sulphate and LAS, the other also contained a silicate binder. Electron density profiles were constructed to quantify the main features of the bilayers: lamellar d-spacings, membrane and hydration water layer thicknesses. Transmission electron microscopy (TEM) was also used to understand whether the lamellar were planar or arranged in vesicles. Furthermore, the effect of changing the relative humidity during storage, and consequently the water activity, on the nano-structural evolution of the lamellae was investigated. This analysis was complemented by FTIR analysis, to further understand the conformational changes of NaLAS hydrocarbon chains in the bilayers and how these change on changing water activity.

## **2. Materials and Methods**

### **2.1 Materials**

Detergent granules were produced with a pilot-scale spray dryer by Procter & Gamble, Newcastle Innovation Centre; detailed information are given in [1]. All spray-dried detergent powders contained the sodium salt of linear alkylbenzene sulphonate (NaLAS), with an average molecular weight of 340 g/mol, and sodium sulphate. Detergent powders containing silicate species were produced by the addition of commercial sodium silicate with the  $\text{SiO}_2:\text{Na}_2\text{O}$  molar-ratio of 1.6 to the detergent slurry. The details of the two compositions are given in Table 1. The resulting detergent powders were then conditioned by storing them in desiccators at a range of relative humidities: 11, 33, 54, and 75%. The relative humidities

were created using saturated solutions of lithium chloride, magnesium chloride, magnesium nitrate hexahydrate and sodium chloride at  $21 \pm 1^\circ\text{C}$  for four weeks.

**Table 1.** Composition of the detergent slurry formulations.

Description	Compositions of the detergent slurries (wt%)			
	Water	LAS	Sodium Sulphate	Sodium Silicate (1.6 R)
Nil-silicate	30	13.6	56.4	
1.6 R	28	14.0	49.3	8.6

## 2.2. Micro-computed tomography (Micro-CT) scanning

The morphology and internal structure of spray-dried detergent granules were qualitatively examined using a Phoenix Nanotom CT scanner (GE Measurement and Control, Wunstorf, Germany). This provides good insight into the distribution of high-, mid- and low-electron density phases within the powder. The high-electron density regions are due to initially undissolved inorganic salts, *i.e.* crystals of sodium sulphate, mid-electron density regions are NaLAS rich and low-electron density regions are pores and vacuoles.

The detergent powders were sieved with 300 and 350  $\mu\text{m}$  mesh size sieves. The individual granules were then mounted on a rotating stage between an X-ray source and X-ray detector. Samples were then scanned and a total number of 1440 angular projections were acquired at  $0.25^\circ$  angular intervals in a single  $360^\circ$  rotation. A series of X-ray micrographs were obtained, and three-dimensional volumes were reconstituted using the VGStudio software package (Volume Graphics GmbH, Heidelberg, Germany). To improve the 3D data visualisation, a number of different image processing tools including filtration and segmentation, were applied to the X-ray micrograph data using the Avizo software 8.0 (FEI,

Oregon, USA). A non-local means filtration was applied to the grey scale projections to reduce image noise. The segmentation of highly dense regions, corresponding to initially undissolved sodium sulphate particles, from the matrix was conducted using an interactive thresholding tool in Avizo.

### 2.3 Small Angle X-ray Scattering (SAXS)

SAXS measurements were carried out using a Xeuss 2.0 SAXS camera system (Xenocs, Sassenage, France). A Cu-K $\alpha$  X-ray source ( $\lambda=0.154$  nm) was used. The scattering angle was calibrated using silver-behenate with the known  $d$ -spacing of 5.84 nm [11]; the scattering vector modulus is defined as  $q = 4\pi \sin(\theta) / \lambda$ , with  $2\theta$  being the scattering angle. Before the radial integration of the 2D-diffraction pattern was carried out (with Foxtrot software developed at SOLEIL, Saint-Aubin, France), the beam-stop shadow, hot pixels, dead pixels and gaps between detector modules of the Pilatus detector (Dectris, Baden, Switzerland) have been masked. From the obtained 1D-data, the diffraction peaks were then fitted with Lorentzian distributions using the Origin 2016 software (OriginLab Corporation, Northampton, MA).

The SAXS data were further analysed by reconstructing electron density profiles (EDP) of the one-dimensional repeat of bilayer stacking by Fourier analysis. Note, in-plane densities along the  $x,y$ -coordinates of the bilayer are not considered, while the electron density contrast,  $\Delta\rho$ , along the  $z$ -coordinate and can be expressed as:

$$\Delta\rho(z) = \sum_{h=1}^{h_{max}} \pm F_h \cos\left(\frac{2\pi zh}{d}\right), \quad (1)$$

where  $h$  is the order of the Bragg peaks,  $z$  is the distance in real-space,  $d$  gives the repeat spacing, and  $F_h$  are the form factors. Note,  $F_h$  were determined by the square-root of the peak intensities,  $I_h$ , having applied beforehand a Lorentz correction of  $h^2$  [12]. The EDP maxima

positions were used to estimate the average distance between NaLAS headgroups, *i.e.* the bilayer thickness,  $d_{HH}$  (see Figure 1b; right). The hydration water layer,  $d_w$ , is then given as  $d_w = d - d_{HH}$ . The following abbreviations are used, throughout this paper, to identify the lamellar phases:  $L_\alpha^M$  and  $L_\alpha^D$ : liquid crystalline lamellar phases enriched with long- and short-chain LAS isomers, respectively;  $L_\beta^M$  and  $L_\beta^D$ : water-poor crystalline lamellar gel phases, enriched with long- and short-chain LAS isomers, respectively.

## **2.4 Transmission electron microscope (TEM) observations**

Microscopic observations on the morphology of liquid crystalline phases were conducted using aberration-corrected TEM (FEI Titan Cubed Themis 300) operated at 300 kV. Prior to microscopic observations, the detergent granules were gently crushed in a mortar. The TEM samples were then prepared by touching the sample side of the copper TEM grid to the milled sample in order to capture a few fine particles of detergent powder.

## **2.5 Attenuated Total Reflectance (ATR)-FTIR measurements**

The infrared spectra were recorded with a Nicolet iS10 FT-IR Spectrometer (Thermo Fisher Scientific, USA) using the ATR method. The detergent powders were mounted on the top of a high-refractive index ATR crystal and then slightly pressed onto it by a pre-mounted sample clamp. The infra-red signal was obtained after being entirely internally reflected in the medium of ATR crystal. Background corrected spectra were measured over a range of 550-4000  $\text{cm}^{-1}$  with 4  $\text{cm}^{-1}$  resolution.

### 3. Results and Discussion

#### 3.1 Small Angle X-ray Scattering measurements (SAXS)

The periodicity ( $d$ -spacing) of lamellar phases ( $L_\alpha$ ,  $L_\beta$ ) was examined by SAXS measurements on samples stored at 33% and 75% RH. Furthermore, detailed structural information, *i.e.* the hydration water layer thicknesses and the hydrocarbon chain lengths were obtained through the determination of the electron density profiles of the bilayer stacking (refer to Materials and Methods section 2.3).

##### 3.1.1 Nil-silicate blown powder

The SAXS patterns of detergent powder obtained from the nil-silicate slurry, containing NaLAS and sodium sulphate, are shown in Fig. 3a. At 33% RH, four different sets of lamellar peaks were detected, showing the presence of multi-lamellar phases differing in  $d$ -spacings (lattice spacings). At higher relative humidity (75% RH) a noticeable change in their SAXS pattern is observed. The peaks at 0.14 and 0.16  $\text{\AA}^{-1}$ , corresponding to relatively long-periodicities of 42.6 and 38.4  $\text{\AA}$ , disappear, leading to two coexisting phases only (Fig. 3a). This is also evident in fewer scattering rings in corresponding 2D SAXS image (Fig. 3d). This was accompanied by an increase in intensity of the Bragg peaks of the remaining phases. The occurrence of multi-lamellar phases of NaLAS is not unexpected, especially for the dried systems studied. They have been observed previously in poly-dispersed, multi-isomer commercial NaLAS solutions [4, 8] and a pure single isomer (Ockelford et al., 1993). In the commercial systems the authors proposed that this is due to the preferential packing of different positional isomers of NaLAS, which leads to the local segregation of LAS isomers within the bilayers. The domains of different compositions are seen to swell to different extents as temperature increases, leading to multiple scattering peaks. At low water contents,

for the NaLAS-H<sub>2</sub>O systems studied by Richards et al., 2007, multiple peaks were observed at water contents of 30% and less and are attributed to multiple liquid crystalline and solid phases. Interestingly, in the pure system, the perhaps unexpected lateral phase separation is thought to be due to a bi-layer interaction potential with attractive forces between the surfactant head groups. Lateral phase separations have also been observed in lipid membranes under dehydration [13]. A likely mechanism for this phenomenon is the difference in repulsive hydration forces between head groups having different hydrocarbon chains, which alters the intra-layer packing density [14, 15].

In the current study, it is highly probable that NaLAS isomers in the lamellar phases, segregate into different alkyl chain length components, as well as different positional isomers upon dehydration during the spray drying process. With decreasing the moisture content of the slurry droplets, the stacks of lamellae are exposed to an increasing osmotic stress due to the difference in water chemical potential between the confined water inside the lamellar structure and surroundings, leading to the dehydration of water layers [16]. As the membranes come into close apposition, repulsive hydration forces acting between opposing headgroups become dominant, inducing a lateral compression stress. The lateral compression stresses have been suggested to be responsible for demixing of membrane constituents and for transitions from liquid crystalline phases to other potential phases [17]. However, the resistance against lateral compression varies across the bilayer, with the molecular arrangement of the alkyl chains and of the surfactant headgroups. In surfactant studies, it has been suggested that surfactants with a “single-like” alkyl chain, *e.g.* 2- and 3-phenyl isomers in the current study, are relatively tightly packed compared with v-shaped molecules, giving rise to a denser headgroup region. The relatively looser packing of the v-shaped tails increases the area per hydrophobic tail, resulting in increased water penetration between the headgroups. This consequently attenuates the headgroup-headgroup interaction, thereby

lowering surface dipole potential [18]. Possibly, these locally different arrangements of the alkyl chains give rise to various levels of compressibility / dehydration across the lamellar structures.

Consequently, the extra pair of peaks at the lower RH can be attributed to the formation of water-poor gel-like phases during the drying process, these are labelled  $L_{\beta}^M$ ,  $L_{\beta}^D$ .

Upon increasing the RH these hydrate and transition to their liquid crystalline counterparts  $L_{\alpha}^M$  and  $L_{\alpha}^D$ . This observation is explained by changes in the alkyl chains' conformation, induced by increased fluidity. The conformation of hydrocarbon chains is defined by an arrangement that can be altered through an internal rotation,  $\tau$ , around the C-C axis of methylene group (-CH<sub>2</sub>) of alkyl chains. A relatively smaller rotation angle for *gauche* conformers ( $\tau = \pm 60^\circ$ ) as compared with *trans* conformers ( $\tau = \pm 180^\circ$ ), cause them to adopt a non-planar structure [19]. In general, the greater the number of the *gauche* conformers, the shorter is the mean length of the hydrocarbon chains [20]. It has been shown that a transition from *trans* to *gauche* conformation in hydrocarbon chains occur under high fluidity of membranes [21, 22]. Transitions from *trans* to *gauche* conformation in hydrocarbon chains will be discussed further in section 3.2.

The pair of peaks, e.g.  $L_{\alpha}^M$  and  $L_{\alpha}^D$ , is attributed to phases with different positional isomer composition, the higher *d*-spacing peaks being rich in 2- and 3-phenyl isomers, with a “single-like” alkyl chain in the bi-layer and the lower *d*-spacing phase being rich in v-shaped 5- and 6-phenyl isomers with “dual-like” alkyl chains in the bi-layer, consequently the super-script M – mono, and D – dual is used to label these phases.

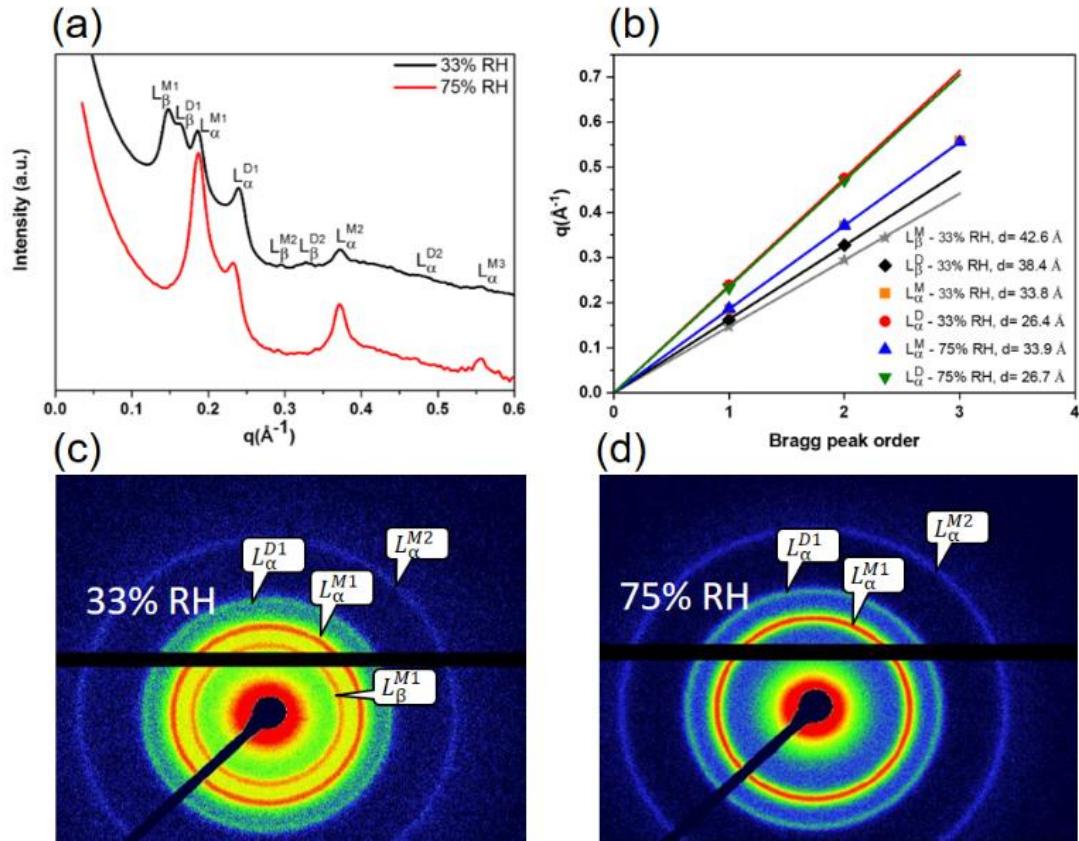


**Figure 3.** (a) SAXS patterns of spray-dried powders produced from the nil-silicate slurry. (b) Shows the lamellar  $d$ -spacings of phases  $L_{\beta}^M$ ,  $L_{\beta}^D$ ,  $L_{\alpha}^M$  and  $L_{\alpha}^D$  as determined from the slopes of Bragg peak position versus peak orders. (c) and (d) illustrate 2D SAXS images of spray-dried detergent powders stored at 33% and 75% RH, respectively.

The curvature of the lamellar phases is also of interest, as both planar (sheets) and spherical (vesicle) morphologies have been observed in similar systems in solution. Farshchi, et al. [1] saw no evidence of vesicles in their analysis of the blown powders, however here that analysis is extended using TEM. A typical morphology of the self-assembled structures can be seen in a TEM micrograph in Fig. 4, showing alternating dark and bright striations associated with the surfactant lamellae along with dark regions attributed to nano-crystallites of sodium sulphate. In the surfactant regions the bright and dark regions correspond to the electron-rich sulphonate head groups and low-electron density hydrocarbon region, respectively. It can be seen that dark layers display relative fluctuations in thickness,

signifying different hydrocarbon chain length, and hence different  $d$ -spacings. Interestingly, the TEM analysis showed no evidence for multi-lamellar vesicle (MLV) structures which have been reported previously in similar but more diluted systems [23-25], only planar packing arrangements of the lamellae were observed in blown powder as shown in Fig. 4.

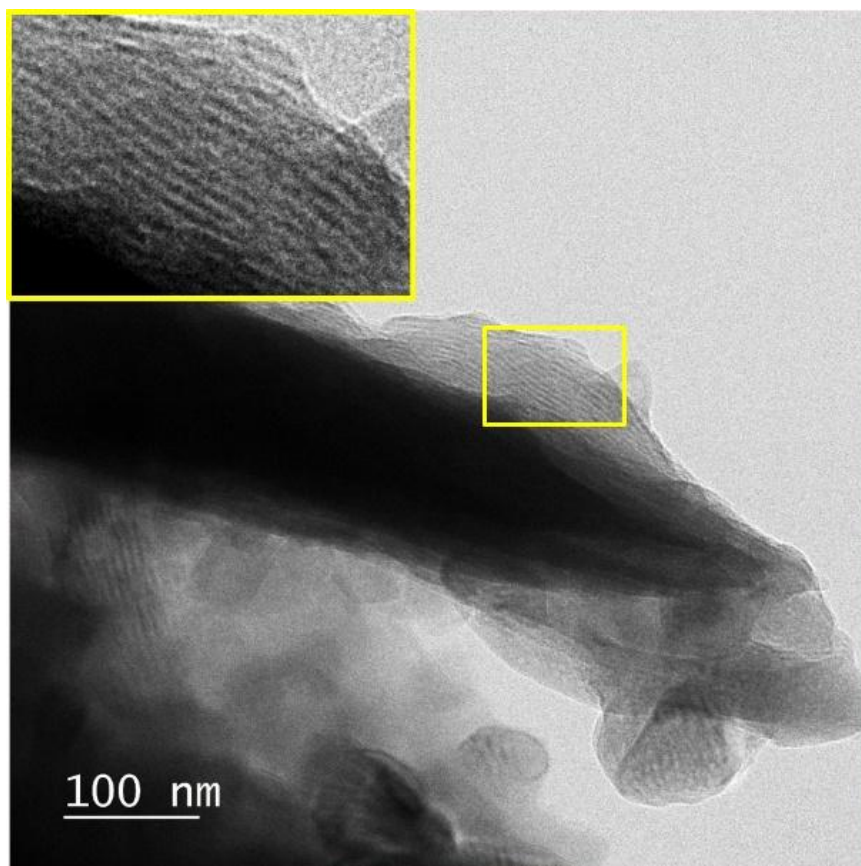


**Figure 4.** TEM micrograph showing a typical multi-lamellar morphology in a nil-silicate detergent granule.

### 3.1.2 Silicate-containing blown powder

Fig. 5a exhibits SAXS patterns from detergent granules containing sodium silicate. The SAXS patterns show two distinct sets of scattering peaks with  $q$  ratios of 1:2 and 1:2:3, with respect to the first order of scattering peaks. This signifies the presence of a relatively uniform lamellar phase containing two co-existing phases with well-defined periodicities.

Interestingly, at 33% RH the scattering patterns are quite similar to those of nil-silicate detergent powders subjected to 75% RH. In other words, the addition of silicate salts into the detergent powders demonstrates similar behaviour to the condition that the relative humidity was increased or higher membrane fluidity was induced in nil-silicate powders. Such behaviour is also observed, when impurities are incorporated within the bilayer structures, which induce more disordered bilayers [26]. It has been suggested that polyhydroxylated compounds can interact with polar headgroups in bio-membranes, possibly through hydrogen bonding, thereby intercalating separating the headgroups. The intercalation of polyhydroxylated molecules between lipid headgroups results in a reduction in dipole potential of the surface membrane which therefore laterally expands the bilayer [27]. The increased membrane fluidity becomes even more evident, once the samples are exposed to a higher humidity level. At 75% RH and in presence of sodium silicate, the two peaks (relevant to  $L_{\alpha}^M$  and  $L_{\alpha}^D$ ) tend to merge; the  $d$ -spacings becoming closer.

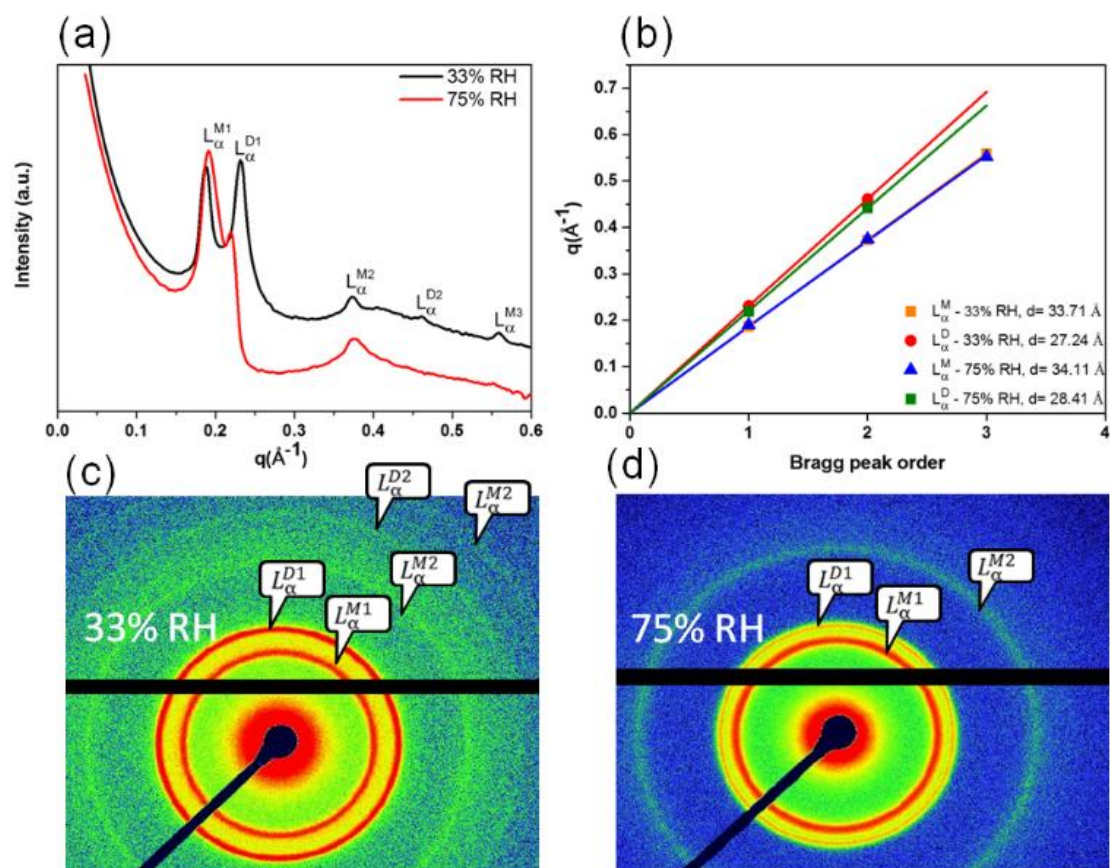


**Figure 5.** (a) Small-angle X-ray scattering (SAXS) patterns of the spray-dried powders containing sodium silicate (1.6  $\text{SiO}_2$ : $\text{Na}_2\text{O}$  R). (b) Shows the lamellar  $d$ -spacings of phases  $L_{\alpha}^M$  and  $L_{\alpha}^D$  as determined from the slopes of Bragg peak position versus peak orders. (c) and (d) illustrate 2D SAXS images of spray-dried detergent powders stored at 33% and 75% RH respectively.

Such trend in destabilising behaviour of the multi-lamellar phases in presence of sodium silicate may be associated to the hygroscopic property of this material, which increases the equilibrium moisture content of the sample at any given relative humidity during the storage. The adsorption and evolution of water layers on hydrophilic silicate species has been demonstrated extensively [28-30]. Further experimental evidence on the effect of increased water content of the salt-incorporated system will be provided later during discussion of the ATR-IR results.

### 3.2. Electron density profiles

In order to quantify the bilayer thickness and the inter-lamellar water layer thickness, Fourier transform reconstructions of electron density profiles were performed as described in the Materials and Methods section. In particular, the  $L_{\alpha}^M$  and  $L_{\alpha}^D$  phases can be used to monitor the structural variations induced by humidity, since these two phases are present at both 33% and 75% RH. Lamellar  $d$ -spacings, membrane thicknesses,  $d_{HH}$ , and the thicknesses of the water layer,  $d_w$  were determined from the electron densities and are listed in Table 2. Table 2. The sulphonate head groups of NaLAS can be identified through the maximum of electron density map due to their close packing on the head group/water interface. The electron-rich head groups are separated by a low-density hydrocarbon region at which the electron density gradually decreases towards the bilayer centre and reaches to its minimum value at  $z = 0$ , where the terminal methyl groups of hydrocarbon chains meet each other (methyl trough region). Also, a more electron-dense region, but yet markedly less than that of head groups, can be observed between the adjacent maxima which is associated with the electron density of the water layer. The bilayer thickness ( $d_{HH}$ ) and water layer thickness ( $d_w$ ) are summarised in the schematics of the lamellar phases in Fig. 6. It can be seen that in phase  $L_{\alpha}^M$  the mean bilayer thickness ( $d_{HH}$ ) reduces slightly from 23.2 Å at 33% RH to 22.9 Å upon exposure to 75% RH, while the size of water layer thickness ( $d_w$ ) remains within errors constant. These results indicate a change from a more ordered to a less ordered lamellar structure with higher membrane fluidity, *i.e.* reflecting a change in the conformation in the hydrocarbon chains displaying more *gauche* conformations upon increased humidity [26, 31]. A similar behaviour is observed for the phase  $L_{\alpha}^D$ : while the bilayer thickness slightly decreases with hydration (increased membrane fluidity), the increase in water layer thickness is more significant resulting in an overall increase in lamellar  $d$ -spacings (Fig. 3b).

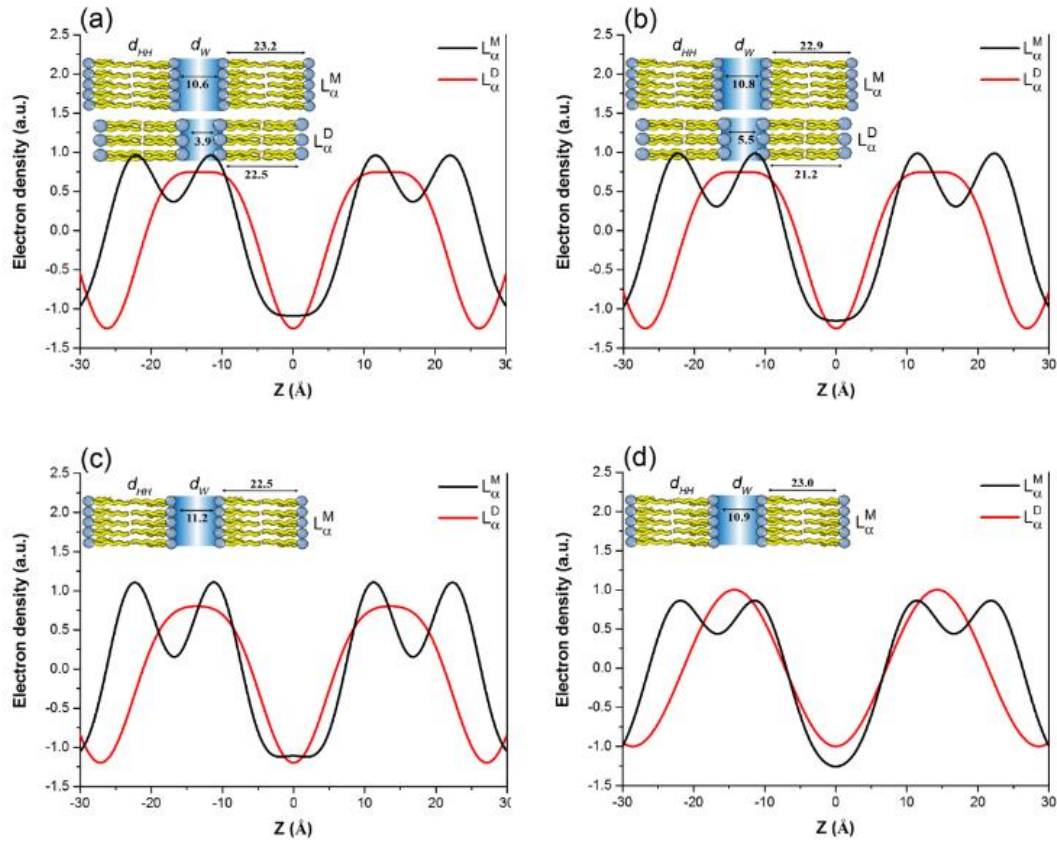


**Figure 6.** The electron density profiles of co-existing lamellar phases. (a) Silicate-free detergent powders stored at 33% RH and their equivalent at 75% RH (b). (c) Silicate-containing powders at 33% RH and 75% RH (d). The electron density profiles calculated from the phase combination of (-1, -1, +1). The electron rich head groups can be detected by the maximum of electron density profiles. The minimum electron density can be found at  $z = 0$  where the hydrocarbon chains meet each other. The parameters of bilayer thickness ( $d_{HH}$ ) and water layer thickness ( $d_W$ ) are summarised in schematics of lamellar phase.

**Table 2.** The parameters of lamellar  $d$ -spacings ( $d$ ), bilayer thickness ( $d_{HH}$ ), water layer thickness ( $d_w$ ) were determined from Fourier analysis of the small angle X-ray diffraction data.

RH	33%	75%
<b>Nil-silicate detergent powders</b>		
$L_{\alpha}^M d_{HH}$	23.2	22.9
$L_{\alpha}^M d_w$	10.6	10.8
$L_{\alpha}^M d$ -spacing	33.8	33.7
$L_{\alpha}^D d_{HH}$	22.5	21.2
$L_{\alpha}^D d_w$	3.9	5.5
$L_{\alpha}^D d$ -spacing	26.4	26.7
<b>Silicate-containing detergent powders</b>		
$L_{\alpha}^M d_{HH}$	22.5	23.0
$L_{\alpha}^M d_w$	11.2	10.9
$L_{\alpha}^M d$ -spacing	33.7	33.9

For silicate-containing detergent powders exposed to 33% RH, the  $L_{\alpha}^M$  phase has similar spacings to the nil-silicate at 75% RH (Fig. 6c and b), though they showed a relatively greater degree of swelling in water layers and a distinct reduction in bilayer thickness as compared with nil-silicate samples. However, in the silicate-containing powder the lamellar phases showed different behaviour when exposed to higher relative humidity. Although, similar to nil-silicate systems, the overall lamellar periodicity of the phase  $L_{\alpha}^M$  increases (from 33.7 to 34.1 Å), the detailed structural information revealed by reconstructed electron density profiles, demonstrate different behaviour. Surprisingly, the  $d_{HH}$  value increases to 23.0 Å and the water layer thickness slightly decreases to 10.9 Å, though this reduction in water layer thickness may fall within a margin of error. These structural changes point out a competitive water absorption between the sodium silicate salt and the multi-lamellar NaLAS nanostructures, which indeed, controls the position of added molecules within the lamellar

structure. We explain this phenomenon as the following. Monomeric species of sodium silicate whether they are located interior or exterior to the inter-lamellar water layers, at low relative humidity (33% RH), play the role of impurity and thus incorporate within the head groups of bilayers, which consequently leads to an increased bilayer swelling. Additionally, the hygroscopic characteristics of sodium silicate increase the equilibrium moisture content of the detergent granules at any given relative humidity, as compared with nil-silicate samples which consequently induces higher membrane fluidity. However, at an increased relative humidity (75% RH), the reason for the reduction of water layer thickness can be explained by the enhanced kosmotropic effect of the polymeric species of sodium silicate, located exterior to the lamellar structures, which competes effectively for the inter-lamellar water molecules. Even though the water layer is expected to increase further at 75% RH, a change in mechanism by which the sodium silicate affects the bilayer interactions leads to actually to a reduction in interlamellar water. This can be explained by a moisture-induced phase transition from a glassy to rubbery state of the polymeric species as a consequence of water plasticisation. This allows a greater number of hydrophilic silanol groups (Si-OH), which are otherwise buried inside the glassy sodium silicate [32], to be exposed to the surroundings which consequently enhances their hygroscopic characteristics [10].

In more detail, polyols are classified as water-structure makers or kosmotropes which have a tendency to order water molecules around themselves leading to a substantial disruption of the tetrahedral order of water molecules [33]. Two main mechanisms have been proposed for these molecules which account for their effects on lipid bilayers. Many studies have suggested that the direct interaction of OH compounds may involve intercalation of bound molecules into the polar head groups which therefore laterally expands the bilayer [15]. Similarly, the provision of hydrogen bonding by sugars, *e.g.* sucrose and glucose, has been demonstrated by Andersen, et al. [34] and Roy, et al. [35]. The authors, however, argued an

additional effect of these compounds which largely arises from their kosmotropic nature by which the osmotic pressure is regulated. It has been hypothesized in multitudes of studies that for instance sugar molecules are excluded from the interfacial region of bilayer membrane. According to the exclusion hypothesis, this gives rise to increasing build-up of osmolytes at the membrane interface, consequently establishing an osmotic gradient and thus extruding water from the bilayers. As a consequence, the head groups may undergo a conformational arrangement by which their effective area is reduced [35, 36]. Andersen, et al. [34] showed that the partial or preferential exclusion effects dominate at high sugar concentrations, while the head group-hydrogen bonding is of significant importance at low concentrations. The authors suggested that these two proposed mechanisms may overlap, and that the overlapping effect can be influenced by the concentration of OH compounds. As discussed earlier, silica species possess hygroscopic characteristics, and are capable of ordering water molecules around themselves [28, 37], which implies their water-structure-making properties. Venugopal, et al. [38] studied the effect of varying concentrations of silica nanoparticles on the phase behaviour of lipid-based lyotropic liquid crystals and showed that lamellar *d*-spacing initially increased, reached a maximum value, with increasing the concentration of silica nanoparticles and then begins to decrease once the concentration exceeds a critical level. This reduction in lamellar *d*-spacing was explained by ordering of the water molecules around silica nanoparticles, which consequently extrudes water from the bilayers.

### **3.3 FTIR measurements**

As discussed earlier, the effect of sodium silicate on the multi-lamellar phases can be two fold at low relative humidity (33% RH). On one hand such binders have been shown to

possess hygroscopic characteristics, thereby favouring the formation of more uniform lamellar phases by enhancing the equilibrium moisture content of the samples. On the other hand, these silicate species are thought to play a role as impurities incorporating within the bilayer head groups. The latter effect can be induced by interactions between silicate species and surfactant head groups through direct hydrogen bonding. In this section ATR-FTIR was used to gain a greater insight into the effects of sodium silicate itself on the structural changes of co-existing lamellar phases. These effects can be primarily studied by probing the vibrational modes of hydrophilic head groups of NaLAS molecules. Infrared spectrum of the detergent powder is presented in Fig 7.

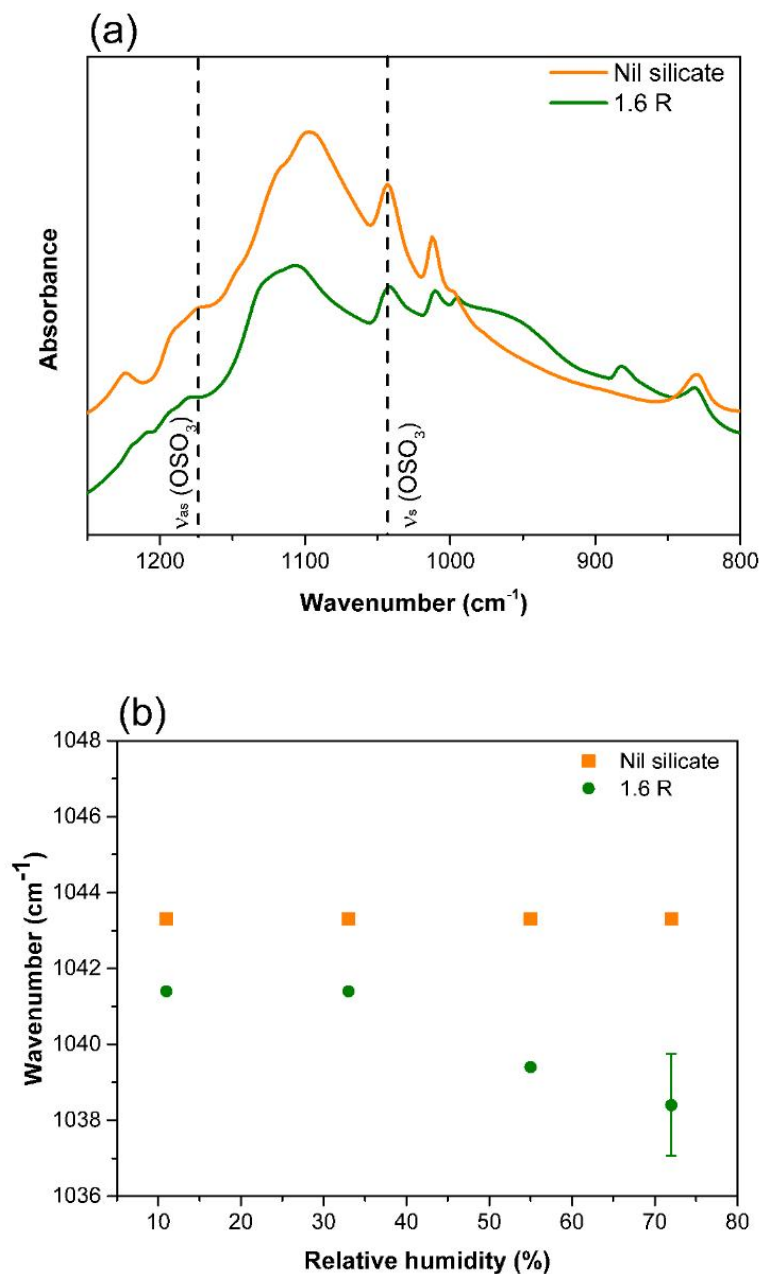


**Figure 7.** (a) Selected region (800-1200 cm<sup>-1</sup>) of ATR-FTIR spectra for spray-dried detergent powders with different formulations at 33% RH. The dashed lines show the symmetric and asymmetric stretching vibrations of S-O bonds in NaLAS. (b) Humidity-induced variations in the wavenumber of the S-O symmetric stretching vibrations in spray-dried detergent powders.

In LAS molecular structure, the sulphonate group,  $-SO_3^-$ , has  $C_{3v}$  symmetry which gives rise to the appearance of two bands around 1040 and  $\sim 1180$  cm<sup>-1</sup>, which are assigned to symmetric and asymmetric stretching vibrations respectively [39, 40]. The bands at 1010 cm<sup>-1</sup>

<sup>1</sup> and  $\sim 1130\text{ cm}^{-1}$  are attributed to aromatic C-H bending vibrations of the benzene ring [39]. As the symmetric stretching band of S-O bonds is well resolved and sharp for all RH values, this mode was chosen to examine changes of hydrophilic head groups as a function of increasing relative humidity. Humidity dependence of this vibrational mode is shown in Fig. 7b for all spray-dried powders.

In the presence of sodium silicate, the peak of the symmetric stretching shifts down in frequency from  $1041\text{ cm}^{-1}$  to around  $1037\text{ cm}^{-1}$  at the highest relative humidity (75% RH), suggesting a distortion of the molecular symmetry. This down-shift in frequency can be explained by the formation of hydrogen bonds between the hydrophilic sulphonate groups and water molecules, as one may expect. It has been suggested that hydrogen bond formation may diminish the strength of S-O bonds, leading to a down-shift in the symmetric stretching band [41, 42]. However, in the absence of sodium silicate, it can be seen that the symmetric stretching mode remains unchanged and no peak shifts was observed even at the largest RH value. This observation was in good agreement with the findings of Boissière, et al. [43] who suggested that the symmetric stretching vibration of S-O bonds is not affected by water layer thickness. The isolated silanol groups (Si-OH) have been shown to have a tendency to interact with polarizable objects such as benzene rings via hydrogen bonding [44]. Evanson and Urban [45] studied the interaction between sodium alkylbenzene sulphonate and acidic copolymers and found evidence for hydrogen-bonding interactions between sulphonate groups of the surfactant and carboxylic groups of copolymers. Therefore, a possible explanation of the noticeable frequency shift can be due to a hydrogen bonding between silanol groups and sulphonate head groups via the path  $\text{S}=\text{O}\dots\text{H}-\text{O}-\text{Si}$ .

Fig. 7b shows a considerably larger downshift in frequency at 55 and 75% RH values indicating a greater degree of hydrogen bonding with sulphonate head groups. These results suggest that at increased levels of relative humidity, more and more silanol groups might

have been exposed to the humid environment, most probably due to a moisture sorption-induced glass transition in amorphous sodium silicate structure [10].

Infrared spectroscopy also provided some good insight into the influence of environmental humidity on the ordering of hydrocarbon chains in liquid crystalline phases. It was earlier demonstrated that hydrocarbon chain domains become shorter as the relative humidity increases. This chain shortening was attributed to the presence of gauche conformers arising from the loosening of the lateral packing of hydrocarbon chains. The influence of relative humidity on the lateral packing and conformational order of hydrocarbon chains can be studied by probing the CH<sub>2</sub> scissoring mode in the 1420-1475 cm<sup>-1</sup> region. When hydrocarbon chains take a monoclinic, triclinic or hexagonal subcellular packing, a singlet can only be observed in this region [46]. However, it is well known that splitting of this mode into two components is a distinguishable signature of orthorhombic hydrocarbon chain packing [47]. Also, the frequency and magnitude of this splitting has been suggested to be associated with the degree of lateral chain packing and side-by-side chain interactions [48]. For crystalline n-alkanes in which all alkyl chains adopt an all-*trans* conformation, this mode is split into two distinct peaks at ~1463 and ~1473 cm<sup>-1</sup> [49].

The vibrational frequencies in the CH<sub>2</sub> scissoring region for the nil-silicate powders can be observed in Fig. 8a. For detergent powders exposed to 11% RH a doublet appeared at 1458 and 1466 cm<sup>-1</sup>. The observed doublet implies that the hydrocarbon chains of lamellar liquid-crystalline phases adopt an orthorhombic-like packing mode where there are two chains per unit cell. This observation is consistent with the X-ray scattering data of nil-silicate powders showing the set of Bragg peaks indicated as  $L_{\beta}^M$  and  $L_{\beta}^D$  at low relative humidity (33%), which were attributed to water-poor gel phases. However, as the relative humidity increased, the lower frequency component of the splitting was less resolved, though the frequencies remained unchanged. These spectral features suggest that the hydrocarbon subcellular

packing in lamellar phases has been distorted because of the weakening of lateral interactions between hydrocarbon chains, and the increases in number of gauche conformers [50]. It was earlier demonstrated that the exposure of nil-silicate detergent powders to 75% RH led to the increasing water layer thickness ( $d_w$ ) and to decreasing the bilayer domain ( $d_{HH}$ ) of the lamellar phase. Therefore, these humidity-induced changes in CH<sub>2</sub> scissoring region support the rationale for the reduction in bilayer thicknesses ( $d_{HH}$ ), which is induced by the increased conformational disorder as a consequence of the swelling and a reduction in lateral attractive interactions between head groups. These structural changes can also explain the disappearance of water-poor gel phases  $L_{\beta}^M$  and  $L_{\beta}^D$ , which are thought to be rich in *trans* conformers, upon exposure to 75% RH.

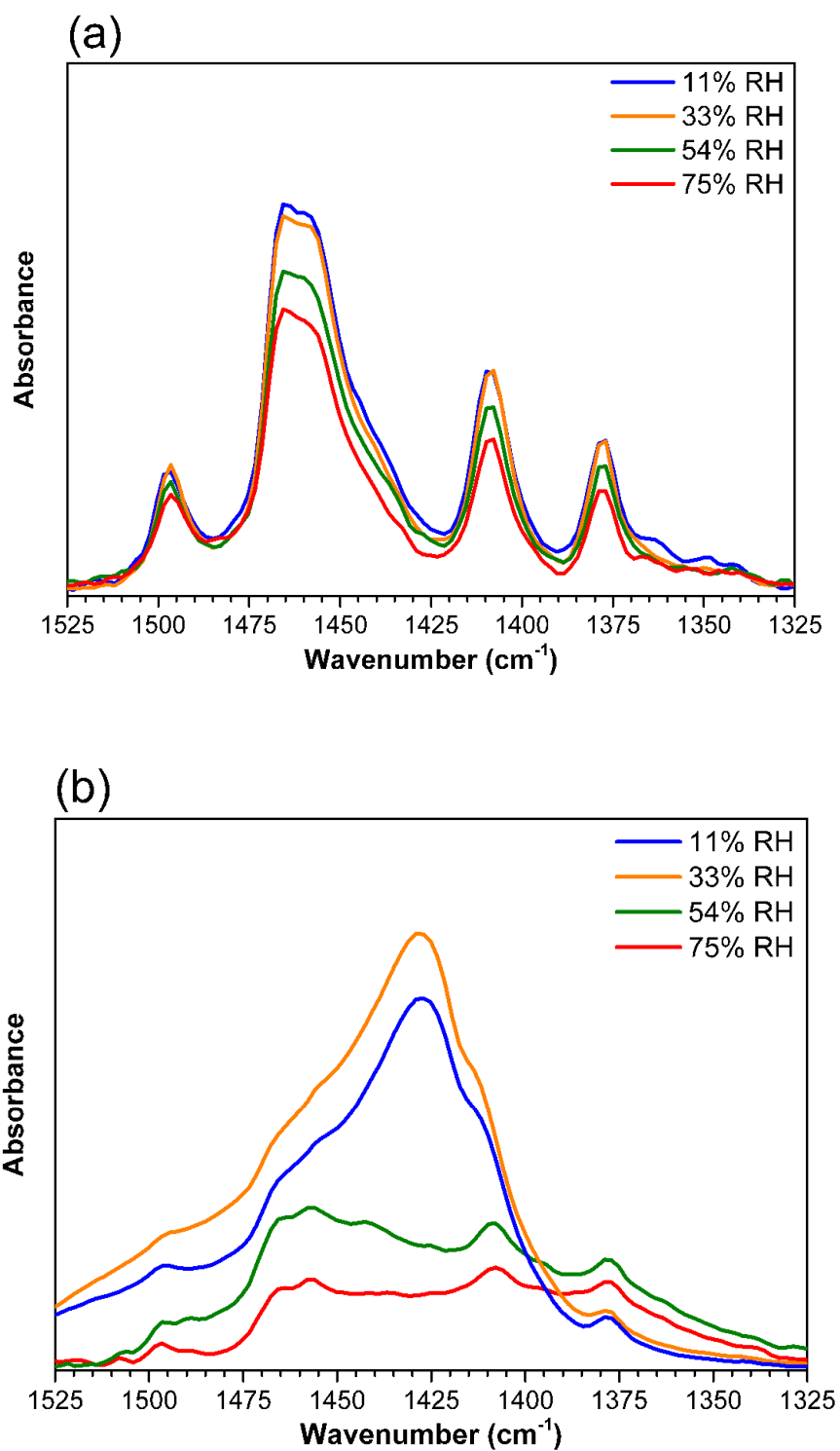


**Figure 8.** (a) Selected region ( $1525\text{-}1325\text{ cm}^{-1}$ ) of ATR-FTIR spectra of the  $\text{CH}_2$  scissoring vibration for nil-silicate detergent powders. (b)  $\text{CH}_2$  scissoring vibration for spray-dried detergent powders containing sodium silicate.

Interestingly, the vibrational behaviour of hydrocarbon chains in the presence of sodium silicate was quite complex. Fig. 8b illustrates the infrared spectra of spray-dried detergent powders containing sodium silicate. It was noticed that at 11% RH, two weak shoulders, which can be the components of the split scissor bands, appear on a sharp peak centred at 1429  $\text{cm}^{-1}$ . At a higher RH value (33% RH), the doublet are more attenuated and are barely discernible. These observations suggest that the hydrocarbon chains are no longer in their perfect arrangement. However, it can be seen that with the increase of relative humidity, the peak at 1429  $\text{cm}^{-1}$  disappeared, while the scissoring doublet at 1458 and 1466  $\text{cm}^{-1}$  became sufficiently well resolved. The presence of an unusual low-frequency band around 1420  $\text{cm}^{-1}$ , within the  $\text{CH}_2$  scissoring region of infrared spectra, was previously reported by Lewis and McElhaney [51] in mixed interdigitated gel phases of phospholipid bilayers, which was attributed to the conformational difference between the esterified acyl chains. However, this subcellular packing mode cannot be readily interpreted due to the existence of a very limited range of known modes for lateral packing of hydrocarbon chains in spectroscopic data [20]. Additionally, in infrared spectroscopic studies of sodium silicate structures, the bands at  $\sim 1430$  have been reported to be due to small amount of adsorbed carbonate formed by the reaction between sodium silicate and  $\text{CO}_2$  in an air atmosphere [29, 52]. Therefore, the nature of this vibrational band cannot be well understood in the current study and merits further investigations.

#### **4. Conclusion**

Four sets of lamellae were detected in spray-dried detergent powders. This was explained by the presence of domains of different compositions, which subsequently dehydrate to different extents upon spray drying, leading to lateral phase separations, and hence formation of multi-lamellar phases. The relative humidity was found to be a critical factor affecting the

coexisting lamellar polymorphs. The exposure of these samples to a high relative humidity level resulted in a reduced number of coexisting phases. This was accompanied by a transition from an orthorhombic-like packing mode of hydrocarbon chains to their less ordered arrangement. As the relative humidity increases, the swelling of lamellar phases results in the shortening of hydrocarbon chains which, therefore, decreases the population of those polymorphs having more *trans* conformers and larger *d*-spacing values. The presence of sodium silicate caused the lamellar phases to swell in a greater degree than those nil-silicate samples, even at a low RH value (33% RH). This was mainly attributed to some sodium silicate species which act as impurities and incorporate within the bilayer head groups, thereby enhancing the water bilayer separation. For these samples, a noticeable reduction in water layer thickness upon exposure to a considerably higher relative humidity value (75% RH) was attributed to the kosmotropic nature of sodium silicate by which the osmotic pressure is regulated. It was hypothesized that a transition from the glassy to rubbery state at such humid conditions may have resulted in the exposure of a greater number of buried silanol groups whereby a larger osmotic gradient is established and thus extruding water from the bilayers.

### **Acknowledgements**

The authors would like to thank the Advanced Manufacturing Supply Chain Initiative (AMSCI) [grant number 31587, 233189] for funding the project. AMSCI is a government supply chain fund which is helping to rebuild British manufacturing processes. We also acknowledge the input of Paul Gould of Procter and Gamble for his support throughout the project.

## References

- [1] A. Farshchi, A. Hassanpour, and A. E. Bayly, "The structure of spray-dried detergent powders," *Powder Technology*, vol. 355, pp. 738-754, 2019/10/01/ 2019, doi: <https://doi.org/10.1016/j.powtec.2019.06.049>.
- [2] P. Alexandridis, U. Olsson, and B. Lindman, "A Record Nine Different Phases (Four Cubic, Two Hexagonal, and One Lamellar Lyotropic Liquid Crystalline and Two Micellar Solutions) in a Ternary Isothermal System of an Amphiphilic Block Copolymer and Selective Solvents (Water and Oil)," *Langmuir*, vol. 14, no. 10, pp. 2627-2638, 1998/05/01 1998, doi: 10.1021/la971117c.
- [3] J.-G. Ma, B. J. Boyd, and C. J. Drummond, "Positional Isomers of Linear Sodium Dodecyl Benzene Sulfonate: Solubility, Self-Assembly, and Air/Water Interfacial Activity," *Langmuir*, vol. 22, no. 21, pp. 8646-8654, 2006/10/01 2006, doi: 10.1021/la0602822.
- [4] J. A. Stewart, A. Saiani, A. Bayly, and G. J. T. Tiddy, "The phase behaviour of lyotropic liquid crystals in linear alkylbenzene sulphonate (LAS) systems," *Colloids and Surfaces A: Physicochemical and Engineering Aspects*, vol. 338, no. 1-3, pp. 155-161, 4/15/ 2009, doi: <http://dx.doi.org/10.1016/j.colsurfa.2008.06.021>.
- [5] J. N. Israelachvili, *Intermolecular and surface forces: revised third edition*. Academic press, 2011.
- [6] Y. Fan and Y. Wang, "Applications of small-angle X-ray scattering/small-angle neutron scattering and cryogenic transmission electron microscopy to understand self-assembly of surfactants," *Current Opinion in Colloid & Interface Science*, vol. 42, pp. 1-16, 2019/08/01/ 2019, doi: <https://doi.org/10.1016/j.cocis.2019.02.011>.
- [7] A. Sein, J. B. F. N. Engberts, E. van der Linden, and J. C. van de Pas, "Salt-induced transition from a micellar to a lamellar liquid crystalline phase in dilute mixtures of anionic and nonionic surfactants in aqueous solution," *Langmuir*, vol. 9, no. 7, pp. 1714-1720, 1993/07/01 1993, doi: 10.1021/la00031a018.
- [8] C. Richards, G. J. T. Tiddy, and S. Casey, "Lateral Phase Separation Gives Multiple Lamellar Phases in a "Binary" Surfactant/Water System: The Phase Behavior of Sodium Alkyl Benzene Sulfonate/Water Mixtures," *Langmuir*, vol. 23, no. 2, pp. 467-474, 2007/01/01 2007, doi: 10.1021/la0617154.
- [9] A. S. Rafique, S. Khodaparast, A. S. Poulos, W. N. Sharratt, E. S. J. Robles, and J. T. Cabral, "Micellar structure and transformations in sodium alkylbenzenesulfonate (NaLAS) aqueous solutions: effects of concentration, temperature, and salt," *Soft Matter*, 10.1039/D0SM00982B vol. 16, no. 33, pp. 7835-7844, 2020, doi: 10.1039/D0SM00982B.
- [10] A. Farshchi, A. Hassanpour, R. Ettelaie, and A. E. Bayly, "Evolution of surface micro-structure and moisture sorption characteristics of spray-dried detergent powders," *Journal of Colloid and Interface Science*, vol. 551, pp. 283-296, 2019/09/01/ 2019, doi: <https://doi.org/10.1016/j.jcis.2019.04.069>.
- [11] T. C. Huang, H. Toraya, T. N. Blanton, and Y. Wu, "X-ray powder diffraction analysis of silver behenate, a possible low-angle diffraction standard," *J. Appl. Crystallogr.*, vol. 26, pp. 180-184, Apr 1 1993, doi: 10.1107/s0021889892009762.
- [12] B. E. Warren, *X-ray Diffraction*. Reading: Addison-Wesley, 1969.

- [13] G. Bryant, J. M. Pope, and J. Wolfe, "Low hydration phase properties of phospholipid mixtures," *European Biophysics Journal*, journal article vol. 21, no. 3, pp. 223-232, July 01 1992, doi: 10.1007/bf00196767.
- [14] G. Bryant and J. Wolfe, "Can hydration forces induce lateral phase separations in lamellar phases?," *European Biophysics Journal*, journal article vol. 16, no. 6, pp. 369-374, February 01 1989, doi: 10.1007/bf00257886.
- [15] E. A. Disalvo *et al.*, "Structural and functional properties of hydration and confined water in membrane interfaces," *Biochimica et Biophysica Acta (BBA) - Biomembranes*, vol. 1778, no. 12, pp. 2655-2670, 12// 2008, doi: <https://doi.org/10.1016/j.bbamem.2008.08.025>.
- [16] F. Nallet, "Surfactant films in lyotropic lamellar (and related) phases: Fluctuations and interactions," *Advances in Colloid and Interface Science*, vol. 247, pp. 363-373, 2017/09/01/ 2017, doi: <https://doi.org/10.1016/j.cis.2017.06.009>.
- [17] C. J. Garvey, T. Lenné, K. L. Koster, B. Kent, and G. Bryant, "Phospholipid membrane protection by sugar molecules during dehydration-insights into molecular mechanisms using scattering techniques," (in eng), *Int J Mol Sci*, vol. 14, no. 4, pp. 8148-63, Apr 12 2013, doi: 10.3390/ijms14048148.
- [18] S. W. Chiu, E. Jakobsson, S. Subramaniam, and H. L. Scott, "Combined Monte Carlo and Molecular Dynamics Simulation of Fully Hydrated Dioleoyl and Palmitoyl-oleoyl Phosphatidylcholine Lipid Bilayers," *Biophysical Journal*, vol. 77, no. 5, pp. 2462-2469, 1999/11/01/ 1999, doi: [https://doi.org/10.1016/S0006-3495\(99\)77082-7](https://doi.org/10.1016/S0006-3495(99)77082-7).
- [19] K. Sato, *Crystallization of Lipids: Fundamentals and Applications in Food, Cosmetics and Pharmaceuticals*. John Wiley & Sons, 2018.
- [20] R. N. A. H. Lewis and R. N. McElhaney, "Membrane lipid phase transitions and phase organization studied by Fourier transform infrared spectroscopy," *Biochimica et Biophysica Acta (BBA) - Biomembranes*, vol. 1828, no. 10, pp. 2347-2358, 10// 2013, doi: <https://doi.org/10.1016/j.bbamem.2012.10.018>.
- [21] T. Hianik, "Structure and physical properties of biomembranes and model membranes," *Acta Phys. Slovaca*, vol. 56, 01/01 2007, doi: 10.2478/v10155-010-0082-z.
- [22] K. Takeda, Y. Andoh, W. Shinoda, and S. Okazaki, "Molecular Behavior of Linear Alkylbenzene Sulfonate in Hydrated Crystal, Tilted Gel, and Liquid Crystal Phases Studied by Molecular Dynamics Simulation," *Langmuir*, vol. 35, no. 33, pp. 10877-10884, 2019/08/20 2019, doi: 10.1021/acs.langmuir.9b01607.
- [23] M. S. Liaw, M. R. Mackley, J. Bridgwater, G. D. Moggridge, and A. E. Bayly, "Multilamellar vesicles in a commercial surfactant system," *AIChE Journal*, vol. 49, no. 11, pp. 2966-2973, 2003, doi: 10.1002/aic.690491126.
- [24] A. S. Poulos *et al.*, "Microfluidic SAXS Study of Lamellar and Multilamellar Vesicle Phases of Linear Sodium Alkylbenzenesulfonate Surfactant with Intrinsic Isomeric Distribution," *Langmuir*, vol. 32, no. 23, pp. 5852-5861, 2016/06/14 2016, doi: 10.1021/acs.langmuir.6b01240.
- [25] S. Khodaparast, W. Sharratt, H. Wang, E. S. J. Robles, R. Dalglish, and J. T. Cabral, "Spontaneous formation of multilamellar vesicles from aqueous micellar solutions of sodium linear alkylbenzene sulfonate (NaLAS)," *Journal of Colloid and Interface*

- Science*, vol. 546, pp. 221-230, 2019/06/15/ 2019, doi: <https://doi.org/10.1016/j.jcis.2019.03.056>.
- [26] B. Drasler, D. Drobne, A. Sadeghpour, and M. Rappolt, "Fullerene up-take alters bilayer structure and elasticity: A small angle X-ray study," *Chemistry and Physics of Lipids*, vol. 188, pp. 46-53, 5// 2015, doi: <https://doi.org/10.1016/j.chemphyslip.2015.04.001>.
- [27] S. R. Al-Ayoubi, P. K. F. Schinkel, M. Berghaus, M. Herzog, and R. Winter, "Combined effects of osmotic and hydrostatic pressure on multilamellar lipid membranes in the presence of PEG and trehalose," *Soft Matter*, 10.1039/C8SM01343H vol. 14, no. 43, pp. 8792-8802, 2018, doi: 10.1039/C8SM01343H.
- [28] D. B. Asay and S. H. Kim, "Evolution of the Adsorbed Water Layer Structure on Silicon Oxide at Room Temperature," *The Journal of Physical Chemistry B*, vol. 109, no. 35, pp. 16760-16763, 2005/09/01 2005, doi: 10.1021/jp053042o.
- [29] T. Uchino, T. Sakka, and M. Iwasaki, "Interpretation of Hydrated States of Sodium Silicate Glasses by Infrared and Raman Analysis," *Journal of the American Ceramic Society*, vol. 74, no. 2, pp. 306-313, 1991, doi: 10.1111/j.1151-2916.1991.tb06880.x.
- [30] S. L. Warring, D. A. Beattie, and A. J. McQuillan, "Surficial Siloxane-to-Silanol Interconversion during Room-Temperature Hydration/Dehydration of Amorphous Silica Films Observed by ATR-IR and TIR-Raman Spectroscopy," *Langmuir*, vol. 32, no. 6, pp. 1568-1576, 2016/02/16 2016, doi: 10.1021/acs.langmuir.5b04506.
- [31] J. F. Nagle and S. Tristram-Nagle, "Structure of lipid bilayers," *Biochimica et Biophysica Acta (BBA) - Reviews on Biomembranes*, vol. 1469, no. 3, pp. 159-195, 2000/11/10/ 2000, doi: [https://doi.org/10.1016/S0304-4157\(00\)00016-2](https://doi.org/10.1016/S0304-4157(00)00016-2).
- [32] H. Roggendorf, M. Fischer, R. Roth, and R. Godehardt, "Influence of Temperature and Water Vapour Pressure on Drying Kinetics and Colloidal Microstructure of Dried Sodium Water Glass," *Advances in Chemical Engineering and Science*, vol. Vol.05No.01, p. 11, 2015, Art no. 53263, doi: 10.4236/aces.2015.51008.
- [33] S. Shimizu and N. Matubayasi, "Gelation: The Role of Sugars and Polyols on Gelatin and Agarose," *The Journal of Physical Chemistry B*, vol. 118, no. 46, pp. 13210-13216, 2014/11/20 2014, doi: 10.1021/jp509099h.
- [34] H. D. Andersen, C. Wang, L. Arleth, G. H. Peters, and P. Westh, "Reconciliation of opposing views on membrane–sugar interactions," *Proceedings of the National Academy of Sciences*, vol. 108, no. 5, pp. 1874-1878, February 1, 2011 2011, doi: 10.1073/pnas.1012516108.
- [35] A. Roy, R. Dutta, N. Kundu, D. Banik, and N. Sarkar, "A Comparative Study of the Influence of Sugars Sucrose, Trehalose, and Maltose on the Hydration and Diffusion of DMPC Lipid Bilayer at Complete Hydration: Investigation of Structural and Spectroscopic Aspect of Lipid–Sugar Interaction," *Langmuir*, vol. 32, no. 20, pp. 5124-5134, 2016/05/24 2016, doi: 10.1021/acs.langmuir.6b01115.
- [36] P. Westh, "Glucose, sucrose and trehalose are partially excluded from the interface of hydrated DMPC bilayers," *Physical Chemistry Chemical Physics*, 10.1039/B806274A vol. 10, no. 28, pp. 4110-4112, 2008, doi: 10.1039/B806274A.
- [37] S. Leroy and M. Wendland, "Simulation of Forces between Humid Amorphous Silica Surfaces: A Comparison of Empirical Atomistic Force Fields," *The Journal of*

- Physical Chemistry C*, vol. 116, no. 50, pp. 26247-26261, 2012/12/20 2012, doi: 10.1021/jp302428b.
- [38] E. Venugopal, S. K. Bhat, J. J. Vallooran, and R. Mezzenga, "Phase Behavior of Lipid-Based Lyotropic Liquid Crystals in Presence of Colloidal Nanoparticles," *Langmuir*, vol. 27, no. 16, pp. 9792-9800, 2011/08/16 2011, doi: 10.1021/la201767p.
- [39] D.-Y. Wang *et al.*, "Structural characteristics and flammability of fire retarding EPDM/layered double hydroxide (LDH) nanocomposites," *RSC Advances*, 10.1039/C2RA20189E vol. 2, no. 9, pp. 3927-3933, 2012, doi: 10.1039/C2RA20189E.
- [40] Z. P. Xu and P. S. Braterman, "High affinity of dodecylbenzene sulfonate for layered double hydroxide and resulting morphological changes," *Journal of Materials Chemistry*, 10.1039/B207540G vol. 13, no. 2, pp. 268-273, 2003, doi: 10.1039/B207540G.
- [41] K. Ohno, M. Fukuda, H. Yoshida, H. Tamaoki, and H. Matsuura, "Vibrational spectroscopic and theoretical calculation studies on conformational behavior of simple sodium 1-alkanesulfonates," *Journal of Molecular Structure*, vol. 553, no. 1, pp. 49-59, 2000/10/10/ 2000, doi: [https://doi.org/10.1016/S0022-2860\(00\)00542-1](https://doi.org/10.1016/S0022-2860(00)00542-1).
- [42] B. Wang, H. Zhang, D. G. Evans, and X. Duan, "Surface modification of layered double hydroxides and incorporation of hydrophobic organic compounds," *Materials Chemistry and Physics*, vol. 92, no. 1, pp. 190-196, 2005/07/15/ 2005, doi: <https://doi.org/10.1016/j.matchemphys.2005.01.013>.
- [43] C. Boissière *et al.*, "Water Confined in Lamellar Structures of AOT Surfactants: An Infrared Investigation," *The Journal of Physical Chemistry B*, vol. 106, no. 5, pp. 1032-1035, 2002/02/01 2002, doi: 10.1021/jp012724i.
- [44] B. Onida, B. Camarota, P. Ugliengo, Y. Goto, S. Inagaki, and E. Garrone, "Mesoporous Benzene-Silica Hybrid Materials with a Different Degree of Order in the Wall Structure: An IR Comparative Study," *The Journal of Physical Chemistry B*, vol. 109, no. 46, pp. 21732-21736, 2005/11/01 2005, doi: 10.1021/jp052754b.
- [45] K. W. Evanson and M. W. Urban, "Surface and interfacial FTIR spectroscopic studies of latexes. I. Surfactant-copolymer interactions," *Journal of Applied Polymer Science*, vol. 42, no. 8, pp. 2287-2296, 1991, doi: 10.1002/app.1991.070420820.
- [46] N. V. Venkataraman and S. Vasudevan, "Interdigitation of an Intercalated Surfactant Bilayer," *The Journal of Physical Chemistry B*, vol. 105, no. 32, pp. 7639-7650, 2001/08/01 2001, doi: 10.1021/jp0105802.
- [47] S. Zhou *et al.*, "Supramolecular complexes: lamellar structure and crystalline transformation," *Polymer*, vol. 45, no. 18, pp. 6261-6268, 2004/08/19/ 2004, doi: <https://doi.org/10.1016/j.polymer.2004.07.019>.
- [48] M. Boncheva, F. Damien, and V. Normand, "Molecular organization of the lipid matrix in intact Stratum corneum using ATR-FTIR spectroscopy," *Biochimica et Biophysica Acta (BBA) - Biomembranes*, vol. 1778, no. 5, pp. 1344-1355, 5// 2008, doi: <https://doi.org/10.1016/j.bbamem.2008.01.022>.
- [49] A. N. Parikh, S. D. Gillmor, J. D. Beers, K. M. Beardmore, R. W. Cutts, and B. I. Swanson, "Characterization of Chain Molecular Assemblies in Long-Chain, Layered Silver Thiolates: A Joint Infrared Spectroscopy and X-ray Diffraction Study," *The*

*Journal of Physical Chemistry B*, vol. 103, no. 15, pp. 2850-2861, 1999/04/01 1999, doi: 10.1021/jp983938b.

- [50] R. N. A. H. Lewis and R. N. McElhaney, "Fourier Transform Infrared Spectroscopy in the Study of Lipid Phase Transitions in Model and Biological Membranes," in *Methods in Membrane Lipids*, A. M. Dopico Ed. Totowa, NJ: Humana Press, 2007, pp. 207-226.
- [51] R. N. Lewis and R. N. McElhaney, "Studies of mixed-chain diacyl phosphatidylcholines with highly asymmetric acyl chains: a Fourier transform infrared spectroscopic study of interfacial hydration and hydrocarbon chain packing in the mixed interdigitated gel phase," *Biophysical Journal*, vol. 65, no. 5, pp. 1866-1877, 1993/11/01/ 1993, doi: [https://doi.org/10.1016/S0006-3495\(93\)81251-7](https://doi.org/10.1016/S0006-3495(93)81251-7).
- [52] W. R. Taylor, "Application of infrared spectroscopy to studies of silicate glass structure: Examples from the melilite glasses and the systems Na<sub>2</sub>O-SiO<sub>2</sub> and Na<sub>2</sub>O-Al<sub>2</sub>O<sub>3</sub>-SiO<sub>2</sub>," *Proceedings of the Indian Academy of Sciences - Earth and Planetary Sciences*, vol. 99, no. 1, pp. 99-117, 1990/03/01 1990, doi: 10.1007/bf02871899.